frontiers in Physics

REVIEW
published: 08 December 2020
doi: 10.3389/fphy.2020.585881

Research on the Influence of Metamaterials on Single Photon LiDAR

*Yingying Hu†, Duoduo Xu†, Zehui Zhou†, Tianqi Zhao *, Yan Shi, Ying Tian, Rui Xu and Yi Chen*

School of Optics and Electronic Technology, China Jiliang University, Hangzhou, China

Single photon light detection and ranging (LiDAR) has the advantages of high angle and distance resolution, great concealment, a strong anti-active jamming capability, small volume, and light mass, and has been widely applied in marine reconnaissance, obstacle avoidance, chemical warfare agent detection, and navigation. With the rapid development of metamaterials, the performance of a single photon LiDAR system would be improved by optimizing the core devices in the system. In this paper, we first analyzed the performance index of the single photon LiDAR and discovered the potential of metamaterials in improving the system performance. Then, the influence of metamaterials on the core devices of the single photon LiDAR were discussed, including lasers, scanning devices, optical lenses, and single photon detectors. As a result, we have concluded that through effective light field modulation, metamaterial technology might enhance the performance innovation of the single photon LiDAR.

Keywords: single photon LiDAR, metamaterial, lidar, light field modulation, enhanced detection

OPEN ACCESS

Edited by:
Chee Leong Tan,
University of Malaya, Malaysia

Reviewed by:
Kun Song,
Northwestern Polytechnical University, China
Lin Chen,
Beijing Radiation Center (BRC), China

****Correspondence:***
Tianqi Zhao
18a0402151@cjlu.edu.cn

†These authors have contributed equally to this work

Specialty section:
This article was submitted to Optics and Photonics, a section of the journal Frontiers in Physics

Received: *21 July 2020*
Accepted: *28 September 2020*
Published: *08 December 2020*

Citation:
Hu Y, Xu D, Zhou Z, Zhao T, Shi Y, Tian Y, Xu R and Chen Y (2020) Research on the Influence of Metamaterials on Single Photon LiDAR. Front. Phys. 8:585881. doi: 10.3389/fphy.2020.585881

1. INTRODUCTION

Inspired by how bats fly, Christian Schuesmaier invented the first radar in the world in 1904. As the combination of traditional radar technology and modern laser technology, light detection and ranging (i.e., LiDAR) is an advanced remote sensing technology, which mainly uses the light reflected from obstacles to determine the actual position information of the target object. Compared with the conventional microwave radar, LiDAR has the advantages of higher angle and distance resolution, greater concealment, stronger anti-active jamming capabilities, better low-altitude detection performance, smaller volume, and lighter mass.

In recent years, LiDAR based on single photon detectors, i.e., single photon LiDAR, has gradually emerged and developed rapidly with the development of single photon detection technologies. With higher detection limit distance and resolution, the single photon LiDAR can achieve multidimensional data, such as azimuth-pitch angle-distance, range-speed-intensity, and display the data in the form of images to obtain radiation geometric distribution images, range-gate images, and velocity images, which has wide applications. First, it is an important means of reconnaissance [1]. For marine reconnaissance, LiDAR was used for the detection and location of water targets [2–5], wave detection [6, 7], and the reconnaissance of sea gas [8]. Then, for land reconnaissance, LiDAR was used for the global monitoring of Earth's ice sheet mass balance [9], aircraft height detection, and topographic surveys [10, 11]. Third, for atmospheric reconnaissance, LiDAR was used for cloud-aerosol detection [12, 13], checking wind speed, and measuring the real-time wind field [14]. For obstacle avoidance, LiDAR promotes the use of driverless cars [8, 15], unmanned ships [16, 17], and

unmanned erial vehicles [18, 19]. Besides, LiDAR can be used for chemical warfare agent detection [20] and navigation [21].

In the following, we analyze the performance index of a single photon LiDAR in section 2, study the influence of metamaterials on a single photon LiDAR in section 3, and finally underline the upcoming prospects for LiDAR in section 4.

2. THE PERFORMANCES INDEX OF SINGLE PHOTON LIDAR

2.1. Measurement Position Accuracy

For LiDAR, the higher the accuracy, the better. The data obtained by LiDAR can be used for obstacle identification, and dynamic object detection and location. If the accuracy is too poor, the above objectives cannot be achieved. However, high precision requires high object configuration requirements, which may have too large a volume. The factors affecting the measurement accuracy include noise, pulse width and time resolution, and the average signal photon number in echo signals.

Noise. The lower the noise, the higher the accuracy of the single photon LiDAR. Reducing the error caused by noise plays an important role in improving the measurement accuracy. The dark count of a single photon detector is a noise contributor which usually causes measurement errors [22]. For the single photon avalanche photodiode (SPAD), a type of single photon detector, the metamaterial integration technology provides a novel way to achieve high photon detection efficiency (PDE), without changing the device structure which obtains low dark counts and good time resolution [23].

Pulse width and time resolution. The pulse width of a laser usually refers to the duration when the laser power is maintained at a certain value. The time resolution of the detector is the minimum recognizable time interval of incident signals. With the increase of pulse width and poorer time resolution, the wider the range of distance statistical discrete distribution is, the lower the measurement accuracy. The pulse shaping technology by metamaterials enables narrower pulse width from the light source.

Average signal photon number in echo signals. When the echo signal is weak, the probability of target detection is low, while the measurement accuracy increases rapidly with the increase of echo signal strength [24, 25]. When the intensity of the echo signal reaches a critical value, the probability of the target detection tends to 1. It is worth mentioning that, compared with traditional SPAD, SPAD with metamaterials on the device surface have the advantage of higher PDE which promote higher probability of the target detection even on the condition of fewer photons in the echo signal. Besides, the meta lens technology could effectively focus photons in the echo signal on the detector.

2.2. Measurement Limit Distance

Different applications have different requirements for the detection range of LiDAR. For example, to be able to detect vehicles ahead on a highway, a telescope needs to be equipped with LiDAR for long-range ranging. The process of pulse laser ranging is generally as follows: launch laser pulse to the target under test, and a time probe for the launch of the laser pulse is recorded. After detecting the echo signal time, the measurement distance is calculated by the basic formula,

$$D = \frac{c \cdot t}{2} \tag{1}$$

where D is the distance between the detector and the detected target; t is the round trip time of laser pulse; and c is the speed of light [26]. The measurement limit distance of LiDAR is dependent on the effective time detection of the echo signal. Therefore, a single photon detector with stronger weak light detection capabilities and good time resolution makes a single photon LiDAR with further measurement limit distance, compared with conventional LiDAR. SPAD integrated with metamaterials is an important approach. Moreover, the vortex beam or polarized laser produced by the metamaterials technology endows the LiDAR system with stronger anti-interference abilities and further measurement limit distance.

2.3. Angular Resolution

Resolution refers to the ability to distinguish between the left and right adjacent targets at a certain distance. The smaller the angular resolution, the smaller the target that can be resolved, so that the measured point cloud data are more delicate. The angular measurement accuracy of general obstacle avoidance LiDAR is only about 0.1°, while the angular resolution of mapping LiDAR is generally 0.001° or even lower. When the mono-pulse method is used to measure the azimuth and pitch angle of the target, the angular resolution mainly depends on the antenna beamwidth and signal-to-noize ratio (SNR) [27]. The wider the beam width is, the stronger the directivity of the LiDAR beam is, and the better the resolution of corresponding direction is. The SNR also affects the resolution and plays an important role for the improvement of the measurement accuracy of diagonal resolution. Therefore, the wider the antenna beam and the higher the SNR, the higher the angular resolution of the LiDAR will be. H igher PDE can be achieved for SPAD integrated with metamaterials, which promotes higher SNR for the single photon LiDAR. In addition, the anti-interference light source and focusing lens realized by metamaterials technology also provides higher SNR.

2.4. Imaging Speed

Most imaging LiDAR uses the imaging technology of single pixel detector LiDAR. The scanning optical system points the transmitting pulse to the target, and the echo intensity reflects the specific reflectivity of the target. The scanner hits the beam at different positions on the target according to a certain scanning pattern, and the image of the target can be obtained through the receiving system. The image speed is usually limited by the scanning speed. Compared with a conventional mechanical scanning method, the laser beam steered by the metamaterials technology provides a possibility of faster scanning.

2.5. Cost

High performance LiDAR with fast imaging speed and long measuring distance, usually requires a lot of hardware with

high cost, including the manufacturing and functional components [28]. Single-photon LiDAR is widely used, such as human eye safety LiDAR [29] and atmospheric signal-to-noize ratio detection in laser remote sensing [30]. A wide range of applications makes the single photon LiDAR more valuable and promotes lower cost. Generally, metamaterial has supernormal physical properties that natural materials do not possess, and it can flexibly adjust and control the phase, amplitude, polarization, and other characteristics of electromagnetic waves through the micro-structure of the subwavelength, as well as being easy to integrate [31]. This means that metamaterial may contribute to the realization of small size, high integration, and low-cost single photon LiDAR.

3. APPLICATION OF METAMATERIAL IN SINGLE PHOTON LIDAR

The core optoelectronic devices in single photon LiDAR are a laser, an optical lens, a scanning device (just for the scanning type LiDAR), and a single photon detector. Because of the development of metamaterials [32–38], the performance of these core devices might be improved.

3.1. Light Source

Making full use of the designed metamaterial can help to effectively regulate the laser light source, such as wavelength, intensity, phase, and polarization. The second-order and third-order nonlinear optical effects in metamaterials have a good application prospect in the field of optical frequency conversion. Through frequency conversion, coherent radiation of various wavelengths can be obtained, which helps to coordinate the light sources of appropriate wavelengths and meet the needs of various practical applications [39]. The nonlinear optical efficiency of the metamaterial is determined by the macroscopic polarization of the metamaterial functional unit and the microscopic polarization of the constituent material. The control of the nonlinear optical field can be realized by designing the material, geometry, and spatial order of the metamaterial functional unit reasonably. It further overcomes the limitations of natural materials in this respect. Compared with 3D metamaterials which are always limited by nano-processing technology and high optical loss, 2D meta-surfaces are easier to process and have relatively low optical loss, so it attracts much attention in the aspect of nonlinear optical field regulation [40]. As a result, the wavelength range limited of the laser light source can be expanded to the ultraviolet and deep ultraviolet area, and make up the cost of expensive laser infrared or ultraviolet light [41–43].

Andrew Forbes demonstrated the first meta-surface laser in the world which produced "super-chiral light": light with super high angular momentum [44]. The new laser produced a new type of high-purity "distorted light" that had never been seen before, including the highest angular momentum reported by the laser. The researchers developed a nanostructured meta-surface that has the largest phase gradient produced to date and allows for high-power operation in a compact design, which is capable of generating a peculiar state of twisted structured light on demand. The meta-surface is composed of many tiny rods of nanomaterials that change the light transmission as it passes through. More importantly, this method is applicable to many laser architectures. For instance, the gain volume and meta-surface size can be increased to produce high-power large volume lasers, or reduce the laser system to a monolithic meta-surface design on the chip.

Based on the principle of linear filtering, the ultrashort pulse polarization can be controlled to a large extent by designing an ultrashort pulse meta-surface, so as to realize the expansion, compression, and remodeling of ultrashort pulse polarization [45]. Since the surface plasmon polaritons (SPPs) can shape the propagating optical spectrum, temporal control of the pulse shape of ultrashort pulses can be achieved through engineered resonances of plasmonic nanoparticles and lattice arrangements. As shown in **Figures 1A,B** a compact ultra-thin plasma meta-surface made of nanoparticles was proposed. Given the input pulses, the meta-surface filter was designed to output the specific pulses with narrower pulse width (**Figure 1C**). And the meta-surface filters are able to compress the different Gaussian pulses with different compression ratios. It is beneficial to realize the optical index of narrow pulse width and high peak power of the laser, thus improving the detection accuracy and broadening the detection range of LiDAR.

The orbital angular momentum shows the potential of improving resolution and an anti-jamming capability [46]. In the propagation process, the vortex beam always maintains the invariability of the hollow distribution, with spin and orbital angular momentum, and the spiral phase structure, which promotes the super-resolution imaging for LiDAR [47, 48]. Jin Han et al. designed and realized an intuitive and simple meta-surface method for generating and manipulating annular vortex beams [49].

The dynamic control of laser output polarization state is an ideal imaging application. Some researchers have used new methods to realize the direct polarization switching of lasers [50]. The laser is integrated with the semiconductor gain medium through a polarization-sensitive meta-surface to amplify the cavity mode and output the polarized laser. The meta-surface is used together with the output coupler reflector. The emitting laser is perpendicular to the outer cavity surface, and the output polarization state can be electrically switched separately. This design means that the laser output has the possibility of high switching speed, compactness, and power efficiency. The use of polarization technology improves the performance of the coherent detection system and promotes the development of high precision LiDAR.

A vertical cavity surface-emitting laser (VCSEL) is a kind of light source with the advantages of low power consumption, low-cost packaging, and ease of fabrication into arrays for wafer-scale testing. Kun Li et. al presented a monolithic, electrically-pumped tunable 1,060 nm VCSELs with a high-contrast grating (HCG) meta-structure as the highly reflective tunable mirror [51], as shown in **Figure 2**. Through electrical actuation of the HCG, the wavelength tuning of larger than 30 nm VCSELs is continuously realized. This is promising for the realization of a high-speed and

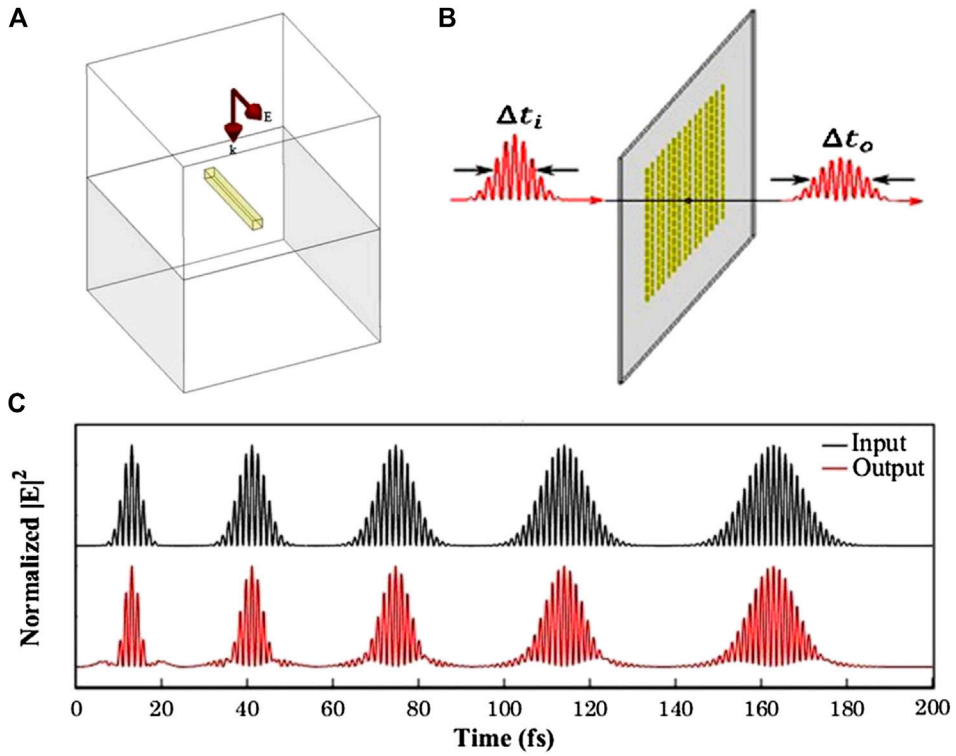

FIGURE 1 | (A) Unit cell of the periodic golden meta-surface on a fused silica substrate with a 2 nm titanium adhesion layer. **(B)** Pulse shaping schematic using a nano-plasmonic filter, which is a periodic golden meta-surface, Δt_i is the half-power pulse width of the input pulse, Δt_o is the half-power pulse width of the output pulse. **(C)** Input/output comparison for different pulse width at the central frequency of 370 THz. *Source*: reproduced from Ref. 45.

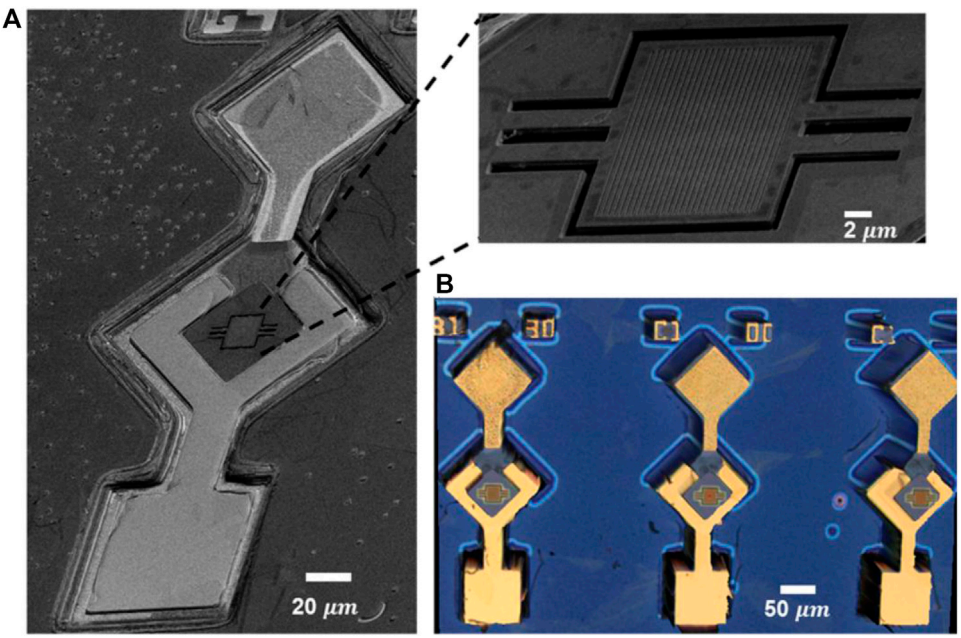

FIGURE 2 | (A) Scanning electron microscope (SEM) image of a typical HCG-VCSEL device, with a zoomed-in view of the fully suspended HCG surrounded by air. **(B)** 3D confocal optical image of the faburicated HCG-VCSEL array. *Source*: reproduced from Ref. 51.

widely variable wavelength tunable source with cost-effective fabrication processes for applications in LiDAR.

3.2. Scanning Structure and Scanning Mode

The space scanning methods of LiDAR can be divided into a non-scanning system and a scanning system [52]. Compared with the traditional mechanical controlling scanning method, the planar devices based on the meta-surface are small and could be easily controlled by the micro-electro-mechanical system (MEMS), which helps to remove the huge components, simplifying the system and lowering the cost [53].

For the non-scanning methods, some researchers have proposed the use of dielectric Huygens meta-surface structures to construct flat lenses and beam deflectors [54]. The device adopts a silicon nano-disk structure to suppress reflection loss. By locally changing the radius of the silicon nano-disk elements, phase transition mutation is realized and arbitrary wavefront control is realized. By experimentally studying the phase gradient, the researchers realized that the plane lens has the characteristic of beam deflection, and the resulting light is similar with that produced by the beam deflection device. Compared with traditional lenses, the design is compact, lightweight, and easier to handle in complex wavefront operations. In addition, controlling the phase and amplitude of light emitted by the elements (i.e., pixels) of an optical phased array is of paramount importance to realizing dynamic beam steering for LiDAR applications. A. C. Lesina presented a plasmonic pixel composed of a metallic nanoantenna covered by a thin oxide layer and a conductive oxide for use in a reflect array meta-surface (as shown in **Figure 3**), which predicted the control of the reflection coefficient phase over a range >330° with a nearly constant magnitude [55]. F. He proposed a silicon surface material that dynamically controls the output light angle [56]. The structure is an array of silicon nanopillars of different diameters with a thick glass substrate underneath. By adjusting the relative phase and intensity of the two incident beams, the angle of output light can be continuous tuned at ~10° as needed. Besides, the output beam has good stability and no distortion, suggesting potential applications in LiDAR.

3.3. Optical System

The function of a LiDAR transmitting optical system is to provide a high power laser, collimate and reshape the beam with an asymmetric shape, produce large divergence and astigmatism

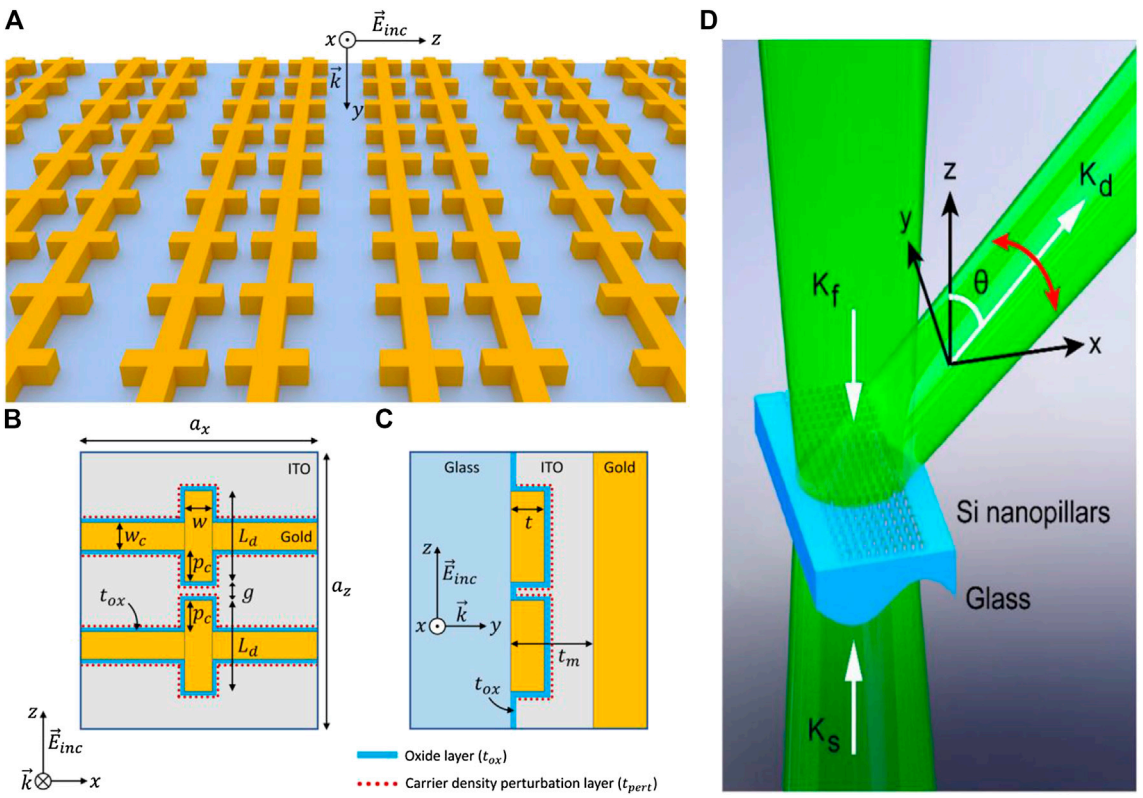

FIGURE 3 | (A) Meta-surface containing an array of plasmonic pixels (only glass substrate and gold nanoantennas are sketched). **(B)** Top view and **(C)** cross-sectional view of the proposed plasmonic pixel. The pixel has dimensions a_x by a_z, and contains a gold dipole nanoantenna which is formed by two branches of length L_d, width w, thickness t, and separated by a gap of size g. The pixel also contains two gold lines of width w_c. The thickness of the meta-surface (metalnanostructure + oxide + ITO) and ITO are denoted as t_m and t_{ox}, respectively. *Source*: reproduced from Ref. 55. **(D)** coherent illumination of a dielectric meta-surface for continuous beam steering. Two counterpropagating light beams (K_f and K_s) illuminate the meta-surface at normal incidence. The propagation angle θ of the output beam (K_d) deflected into free space can be continuously steered via adjusting the relative phase and intensity of the two incident beams. *Source*: reproduced from Ref. 56.

from the semiconductor laser, enhance the echo signal, improve signal-to-noize ratio, and measure the accuracy of the system [57]. The core element of the optical system is a different kind of lens. Because metamaterials can control electromagnetic waves arbitrarily, more attention has been paid to them. A metamaterial lens is one of its typical implementations [58]. Metamaterials can theoretically achieve arbitrary permittivity and permeability. When the electromagnetic impedance of the plate and vacuum is almost equal, it will reflect little electromagnetic waves, while the plate medium will not absorb electromagnetic waves at this time, which means that the conditions for lenses are available. In 2014, D. M. Lin proposed a medium-graded meta-surface optical lens, and successfully realized the production of gratings, lenses, and axicons on the SOI substrate, with the working band in visible light [59]. Using titanium dioxide "nanowires" with about 600 nm height, F. Capasso created a perfectly "flat" paper-thin "focusing lens" [60], as shown in **Figures 4A–F**. The metamaterial lens had an effective magnification of up to 170 times and had an excellent imaging resolution. It used nano-bricks stacked in an unusually neat arrangement with a negative refractive index. By changing the shape, size, and arrangement of the nanostructures (smaller than the wavelength of light), the light can be focused. In addition, a broadband achromatic dielectric meta lens was developed to eliminate the chromatic aberration, which can focus the entire spectrum with wavelengths over 1,200–1,650 nm at the same point (**Figures 4G,H**) [61].

By designing the meta-surface, the distribution of the phase, polarization, and intensity of the spatial light field is controlled locally by a thin layer of the subwavelength structure unit. It can effectively regulate the propagation property of light and expand the means and methods of people's regulation of the electromagnetic wave, so that the development of electromagnetic wave regulation device tends to be miniaturized, planarized, and conformed, and thus has an important application prospect. Huygens' principle and Fermat's principle can be used to calculate the phase distribution required by the metamaterial lens. An optical zoom method based on the wavelength regulation of the metamaterial lens was presented and the tomographic imaging method of the superstructure lens based on the elimination of spherical aberration was realized [62, 63]. However, once the micro-nano structure integrated on the metamaterial lens is prepared, it is usually difficult to change

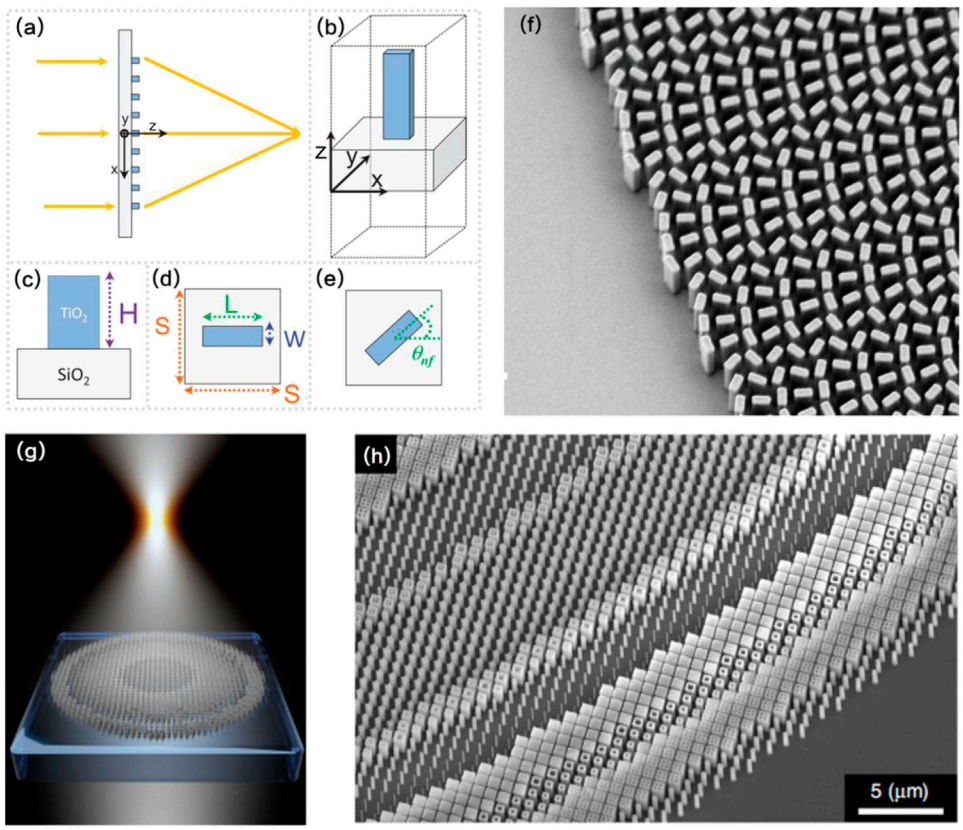

FIGURE 4 | (A) Schematic of the meta lens and its building block, the TiO_2 nanofin. **(B)** The meta lens consists of TiO_2 nanofins on a glass substrate. **(C,D)** Side and top views of the unit cell showing height H, width W, and length L of the nanofin, with unit cell dimensions S × S. **(E)** The required phase is imparted by the rotation of the nanofin by an angle θ_{nf}, according to the geometric Pancharatnam-Berry phase. **(F)** SEM micrograph of the fabricated meta lens. *Source*: reproduced from Ref. 60. **(G)** Schematic of a broadband achromatic meta lens composed of meta-units with complex cross sections, showing dispersionless focusing. **(H)** SEM images of fabricated meta-lenses using meta-units. *Source*: reproduced from Ref. 61.

its morphology or size, so it is impossible to control its focusing performance in real time. Recently, scientists have explored many ways to realize real-time regulation of the focusing performance of a superstructure lens, among which the most striking one is the combination of intelligent materials and a superstructure lens [64]. For example, K. Chen et al., invented a real-time local reconfigurable source Huygens meta lens in the 6.9 GHz working wave band [65], which, to the best of our knowledge, demonstrates for the first time that multiple and complex focal spots can be controlled simultaneously at distinct spatial positions and reprogrammable in any desired fashion, with a fast response time and high efficiency, as shown in **Figure 5**.

In the cases discussed above, the metamaterials give optical lenses the potential to push the limits and even disrupt things like camera lenses. In the future, camera lenses by metamaterials may become as thin as paper, and there will no longer be the inherent distortion and edge image attenuation problems of "convex lenses". Moreover, the lens cost of metamaterial lenses is much cheaper than that of traditional glass lenses, which is an extremely significant development for the industry. However, it is not without flaws. Currently, metamaterials usually regulate electromagnetic waves in a narrow band, which is determined by its principle. Although super lenses can realize sub-wavelength imaging, it has the great requirement for medium loss and absorption [66]. It has also been difficult to develop negative refractive index metamaterials, for the use in optical devices [67].

3.4. Single Photon Detection System

The single photon detector is the core device used for echo signal detection in a single photon LiDAR system. The main kinds of single photon detectors include photomultipliers (PMT), SPADs, and superconduct nanowire single photon detectors (SNSPD). Compared with the fragile PMT with high bias, SPAD has high quantum efficiency, small volume, low bias voltage, and low environmental requirements. SNSPD is a new technology developed in recent years, with a wide spectral response range, a high count rate and time resolution, and very low noise, which is applied in quantum communications. However, SNSPD has to work at a superconducting temperature (<4 K), which needs high-power mechanical refrigeration or liquid helium refrigeration. These supporting refrigeration devices have greatly increased the cost and volume, limiting the large-scale application. Therefore, SPAD is the mainstream single photon detector for LiDAR. However, the photon detection efficiency (PDE) of SPAD is not ideal. For example, the PDE of silicon-based SPAD is not with in the near-infrared wavelength, which limits the detection performance in the application of LiDAR. Recently, SPAD integrated with nano-structures was presented to overcome this drawback. SPAD integrated with a meta-surface not only performs well in PDE, but also holds other SPAD performance metrics well, such as dark count rate, after the pulse, and time resolution. Regardless of the influence of PDE on device structure, the SPAD structure can be independently designed to achieve low dark count rate and good time resolution. Therefore, meta-surface integration is a revolutionary technology

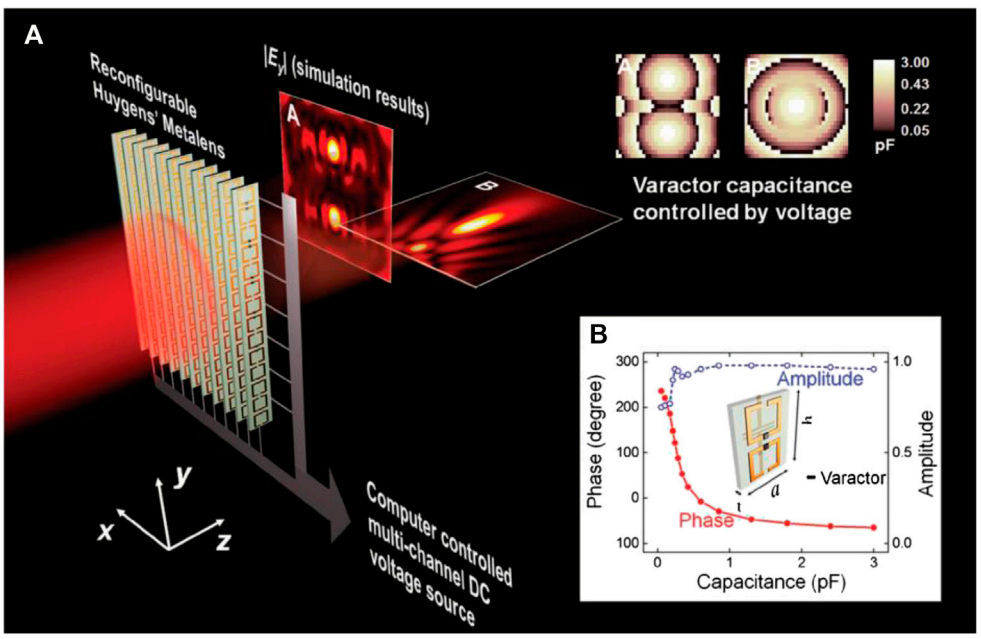

FIGURE 5 | Reconfigurable Huygens' meta lens and characteristics of meta-atom. **(A)** Active Huygens' meta lens for dynamic EM wave focusing, of which meta-atoms are biased by computer-controlled multichannel DC voltage sources. Upper-right inset: spatial distributions of capacitances used to achieve two focal spots either in *x*-*y* **(A)** or in *x*-*z* planes **(B)** based on full-wave simulation. **(B)** Capacitance-dependent phase and amplitude responses of EM wave transmission at the target frequency of 6.9 GHz for incident electric and magnetic fields which are parallel to *y*- and *x*-axes, respectively. *Source*: reproduced from Ref. 65.

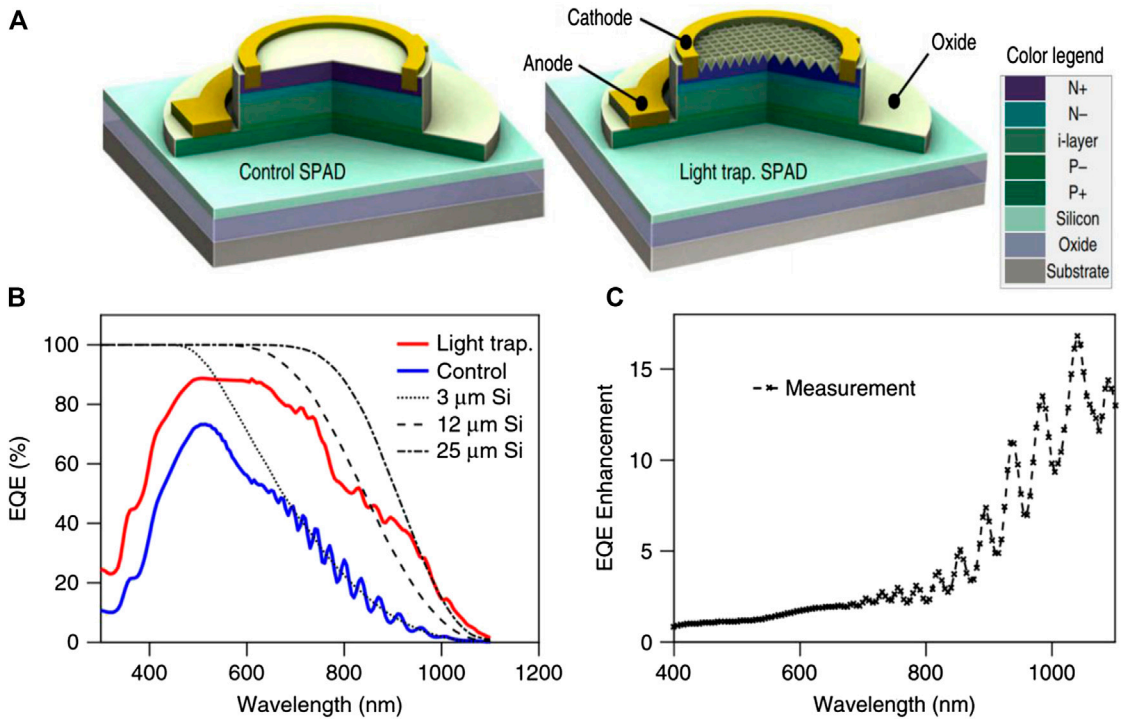

FIGURE 6 | (A) Three-dimensional (3D) cross-sectional schematics of layer configurations of control (left) and light-trapping SPADs (right). **(B)** EQE measurements of control (blue solid) and light-trapping SPADs (red solid); dashed black lines correspond to theoretical absorption of 3, 12, and 25 μm thick Si from left to right. **(C)** EQE enhancement: ratio of light-trapping SPAD EQE compared to control SPAD. *Source*: reproduced from Ref. 68.

for the development of SPAD. There are many kinds of meta-surface, including the inverse pyramid nano-structure array [68], nano cone array [69], nano pyramid array [70], nanowire arrays [71], nano dimples or convex balls array structure [72], and nanosphere shell structure array [73].

As an example of an inverse pyramid nano-structure array, a light-trapping SPAD with a typical mesa-type shallow-junction was fabricated using a complementary metal oxide semiconductor (CMOS) compatible process. Si epitaxial layers with a total thickness of 2.5 μm were grown on an SOI substrate. As shown in **Figure 6A**, the nano-structure was etched as an inverse pyramid, with an 850 nm period in a square lattice pattern. Unlike the resonance peaks found in the responsivity of resonant-cavity-enhanced (RCE) detectors, the light-trapping SPAD has broadband responsivity enhancement. The improvement of external quantum efficiency (EQE) is mainly due to the

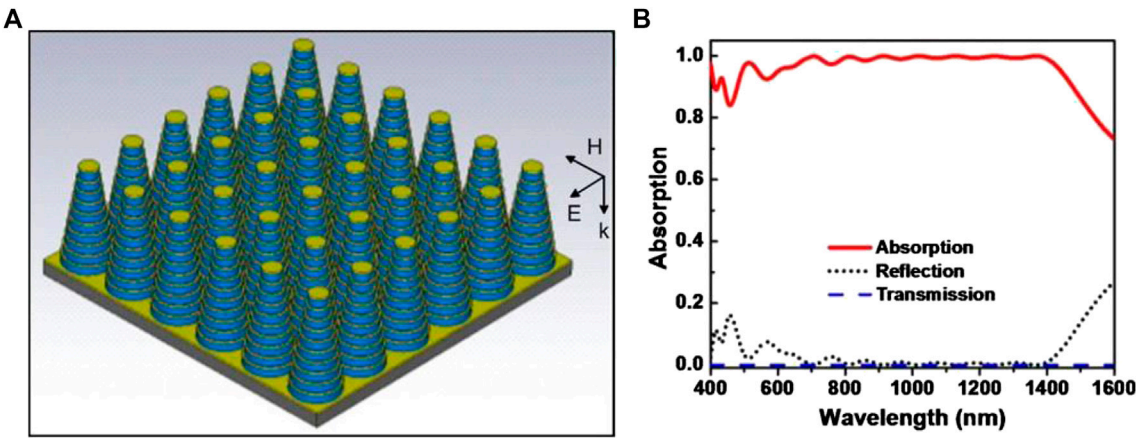

FIGURE 7 | (A) Schematic diagram of truncated cone-shaped metamaterial absorber. **(B)** The reflection, absorption, and transmission characteristics of the absorber. *Source*: reproduced from Ref. 74.

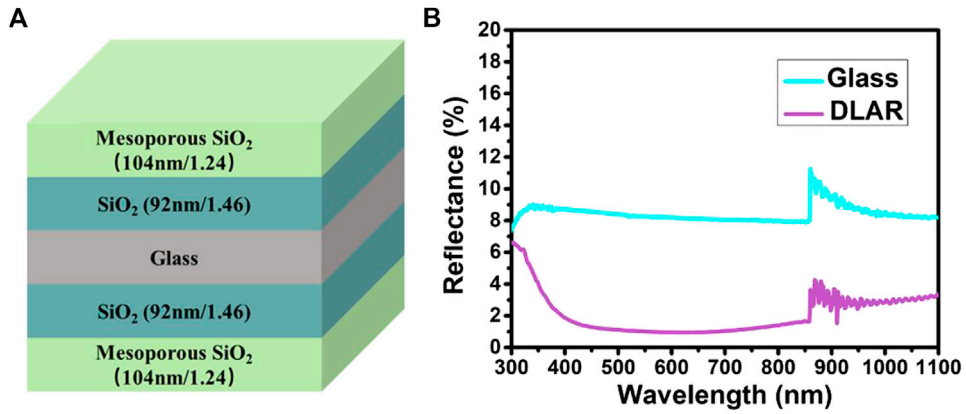

FIGURE 8 | (A) Structure of mesoporous DLAR coating. **(B)** Reflectance spectra of glass and DLAR coatings. *Source*: reproduced from Ref. 75.

enhanced anti-reflection effect and nano-structure diffraction [68]. As shown in **Figures 6B and 6C**, the enhancement effect of EQE is more obvious for longer wavelengths.

A truncated cone-shaped metamaterial absorber was designed using silicon and gold [74], as shown in **Figure 7**. This absorber can achieve an absorption bandwidth of 1,000 nm in the visible and near-infrared bands covering 480–1,480 nm. The material is a kind of multi-layer truncated cone, composed of metal dielectrics (such as gold and silicon) stacked with ultra-wideband metamaterial absorption structures arranged periodically. The number and diameter of the truncated cones in each basic unit are adjusted, and the width of the absorption band can be changed as needed. Through the interlayer exchange coupling of the electric field and the magnetic field in adjacent unit cells, the absorption efficiency can be improved. Under any severe conditions, the receiver has strong stability, the high absorption rate can still remain unchanged, and has good performance in terms of compact structure, large bandwidth, and polarization insensitivity.

Xu et al. presented a mesoporous double-layer antireflection (DLAR) coating [75]. The coating has good performance of high light transmittance and durability. It is a new type of layered structure, as shown in **Figure 8A**. The top silicon layer structure is composed of mesoporous dioxide with a pore diameter of 2–50 nm. The team prepared a metamaterial DLAR coating with an average transmittance of 99.02% in the visible light band from 380 to 780 nm (**Figure 8B**). In addition, the high porosity of the structure is conducive to obtaining a lower refractive index, which can harvest higher transmittance. With another layered structure, M. I. Fathima proposed a theoretical design of Effective Interface Antireflective coating (EIARC) which is based on the theory of Fabry-Perot-Interference filters [76]. In the anti-reflection coating, photons can be reflected multiple times to minimize reflection loss. This design is a combination of a spatial index layer and two multi-layer subsystems.

Zeng et al. designed a nanostructure fabricated by reactive ion etching (RIE) and wet etching on the surface of silicon [77]. The surface of the nanostructure is uneven, which produces multiple reflections on the surface, and forms an effective light-harvesting structure in the 300–800 nm band. As shown in **Figure 9**, the reflectivity of the nanostructure surface by wet etching (Pyramid sample) or RIE (Sample 20) is obviously lower than the blank surface. And sample 22 produced by wet etching and then RIE obtains the minimum reflectance of only 1.27%. W. Chen et al. further improved the anti-reflective properties of the nanostructures by changing reactive gas compositions comprising chlorine (Cl_2), sulfur hexafluoride (SF_6), and oxygen (O_2) for the RIE process [78].

Except physical processing technology, Chen-Chih Hsueh et. al fabricated uniform silicon nanowire (SiNW) arrays on the mono- and multi-crystalline wafers by employing the improved solution-processed metal-assisted chemical etching (MacEtch) method [79]. They demonstrated a good optical trapping effect and reflectance well below 6% over a broad wavelength range from 300 to 1,100 nm with good uniformity, as shown in **Figure 10**. The improved MacEtch concept is suitable for commercial mass production. However, it suffers from a lower effective lifetime, because the higher surface state causes higher surface recombination for the SiNW arrays wafer.

4. PROSPECT

The metamaterials technology promotes the development of the core devices of single photon LiDAR. First of all, the outstanding anti-reflective properties of the meta-surface promoted the development of SPAD with better performance matrix. The meta-surface could flexibly regulate the amplitude and phase of incident light through the subwavelength microstructure, so it has great application potential in the field of beam emission. An optical meta-surface uses the phase mutation of transmitted or reflected waves on the structural surface to effectively regulate the wave front of the incident wave, which can realize the regulation of beam deflection and polarization. In the future, the optical meta-surface could be further used to adjust waveforms to optimize beam transmission, laser amplification and frequency control, and conduct beam shaping to improve beam near-field control ability. Besides, the metamaterial lenses reveal an new industry development direction.

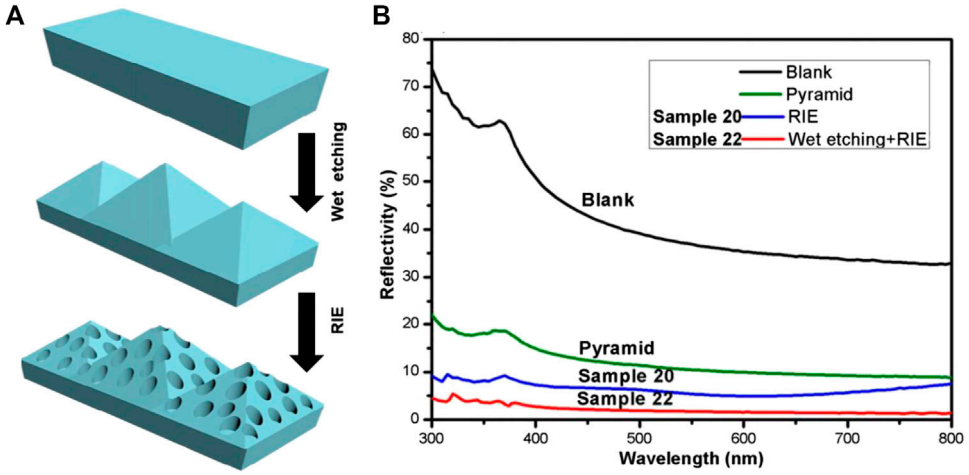

FIGURE 9 | (A) The surface of silicon etched by wet etching and RIE. **(B)** Reflectivity of different kinds of silicon surface. *Source*: reproduced from Ref. 77.

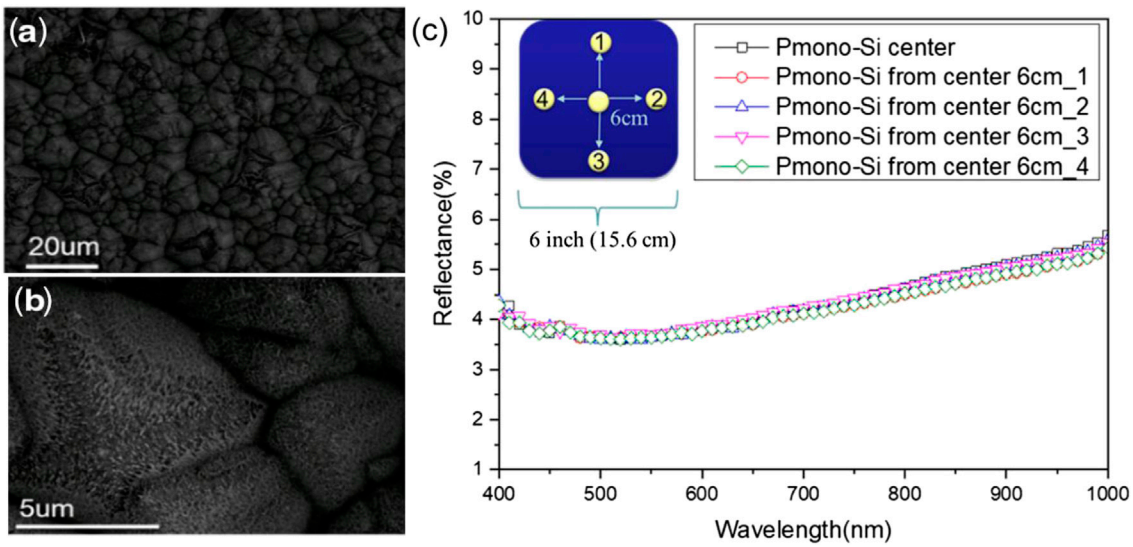

FIGURE 10 | (A,B) Pyramid/SiNW array structure on a P-type mono-crystalline wafer (top view of SEM images). **(C)** Total reflectance of different spots of 6-inch P-type mono-crystalline pyramid/SiNW array structure wafer. The inset marks the measured area at the center and 6 cm from the center. *Source*: reproduced from Ref. 79.

AUTHOR CONTRIBUTIONS

TZ is the corresponding author of the article, who lead this scientific research work and paper writing. YH contributed to the study of the performance index of single photon LiDAR, and the application of metamaterial in lenses. DX contributed to the study of the introduction and prospect part of the paper, and the application of metamaterial in lasers. ZZ contributed to the study of the basic architecture of LiDAR, and the application of metamaterial in scanning devices. YS partly contributed to the writing of the introduction of this paper (Section 1). RX partly contributed to the writing of the performance index of single photon LiDAR (Section 2). YC partly contributed to the writing of the application of metamaterial in single photon LiDAR (Section 3). YT partly contributed to the writing of the prospect part of the paper (Section 4).

FUNDING

This work was supported by the National Key R&D Program of China (Grant No. 2018YFF0215304), the National Nature Science Foundation of China (NSFC) (Grant Nos. 61904169 and 61904168), the Zhejiang Provincial Natural Science Foundation of China (Grant No. LQ18F040001), the Technique Support Program of State Administration for Market Regulation (No. 2019YJ067), and the Major Scientific Research Project of Zhejiang Lab (2019DE0KF01).

REFERENCES

1. Hou Y, Li D, Kong X, Chen S. Integrated electronic warfare-an assassin's mace in modern warfare. Beijing, China: National Defense Industry Press (2000) 56 p.
2. Nong G, Yue Y, Yang G, Sun W. Applications of satellite observation information in ocean surveillance and reconnaissance. *Ship Sci Tech* (2011) 144(z1):92–5. doi:1672-7649 (2011) S-0092-04
3. Zhang L, Liu Z, Li G, Cheng-Wen Z. Research on a new method of moving target positioning by reconnaissance missile at sea-taking compass+PD/HRLR combination as foundation. *Opt Optoelectron Technol* (2013) 11(4):77–81. doi:CNKI:SUN:GXGD.0.2013-04-017
4. Mingtao Z, Zhang J, Zhang J, Hang X, Mingjiang Z, Wang A, et al. Chaotic modulation lidar for underwater ranging. *Laser Optoelectron Prog* (2016) 53(5): 232–9. doi:10.3788/LOP53.051402
5. Fu C, Fang L, Xie L, Wang Y. Prototype design and water-land joint survey test of airborne dual-frequency lidar. *J PLA Univ Sci Tech* (2016) 17(6):520–5. doi:10.12018/j.issn.1009-3443.20160425003
6. Liu C, Mao Q, Chu X, Xie S, Wang F, Yan B. *The invention relates to a shipborne wave dynamic measuring device based on lidar*. CN109490906A (2019).
7. Jian H. *Research on detection of submarine through short scale ocean waves using a streak tube imgaging LiDAR*. Harbin, China: Harbin Institute of Technology (2014)
8. Wang C, Kong B, Yang J, Wang Z, Zhu H. An algorithm for road boundary extraction and obstacle detection based on 3D Lidar. *Pattern Recognit Artif Intell* (2020) 33(4):353–62. doi:10.16451/j.cnki.issn1003-6059.202004008
9. Yu A, Stephen MA, Li SX, Shaw GB, Seas A, Dowdye E, et al. Space laser transmitter development for ICESat-2 mission. *Proc SPIE* (2010) 7578:757809. doi:10.1117/12.843342
10. He S. *Linear light source terrain detection Sharm lidar*. CN207037090U (2018)
11. Qu S, Zhang X, Zhu C, Huo L, Liu H. Design and test of airborne LiDAR system for forest resources survey. *J Northwest For Univ* (2018) 33(4):175–82. doi:10.3969/j.issn.1001-7461.2018.04.29
12. Shangyong G, Xiong H, Zhaoai Y, Yongqiang C, Wenjie G, et al. Research development of space-borne lidar in foreign countries. *Laser Technol* (2016) 40(5):772–8. doi:10.7510/jgjs.issn.1001-3806.2016.05.032
13. Wu D, Wang J, Yan F. Estimation of air-sea gas transfer velocity using the CALIPSO lidar measurements. *Acta Opt Sin* (2012) 32(9):270–8. doi:10.3788/AOS201232.0928001
14. Shen F, Sun D, Wang Z, Xianghui X, Tingdi C, Xiankang D. Beam scanning and wind inversion technique of a Mobile Doppler Lidar. *Acta Opt Sin* (2012) 32(3):1–5. doi:10.3788/AOS201232.0312004
15. Zhang N, Bao X, Li H. Intelligent vehicle obstacle recognition based on lidar and camera fusion. *Sci Technol Eng* (2020) 20(4):1461–6. doi:CNKI:SUN:KXJS.0.2020-04-025
16. Zuang J, Jiao N, Yin F. Application of MMW radar and lidar in mass. *Ship Eng* (2019) 41(11):79–82. doi:10.13788/j.cnki.cbgc.2019.11.15
17. Bi X. *Lidar-based unmanned ship slam obstacle avoidance technology*. Dalian, China: Dalian Maritime University (2019).
18. Lai W, Liu Z, Ji K, Xu L, Zhang B. System design of autonomous patrol UAV based on lidar. *Microcontrollers Embedded Syst* (2020) 20(5):37–40. doi:CNKI:SUN:DPJY.0.2020-05-012
19. Quan Y, Li M, Zhen Z, Yuanshuo H. Modeling crown characteristic attributes and profile of larix olgensis using UAV-borne lidar. *J Northeast For Univ* (2019) 47(11):52–28. doi:10.13759/j.cni.dlxb.2019.11.011
20. You W, Chen D, Zeng Q. Research status of chemical warfare agent remote detection system in air force airfield. Proceedings of the 5th chemical prevention symposium of the Chinese Chemical Society. Kunming, China: Chinese Chemical Society (2001). p. 571–5.
21. Liu L, Cai X, Qiao L. Research of active imaging guiding lidar system. *Infrared Laser Eng* (2000) 29(2):36–40
22. Wu J, Pu G, Shen H, Yang X, Bu X. Analysis and research of laser ranging technology based on core instruments detection of SPAD. *Laser J* (2019) 40(9): 29–33. doi:10.3969/j.issn.1007-2276.2014.02.008
23. Ma J. *Design of single photon avalanche diodes*. Hefei, China: University of Science and Technology of China (2016).
24. Liu C, Chen Y, He W, Gu G, Chen Q. *Simulation and accuracy analysis of single photon ranging system*. *Infrared Laser Eng* (2014). 2(6):382–387. doi:10.3969/j.issn.1007-2276.2014.02.008
25. Zeng X, Song L, Wang J. *Detection simulation of dangerous space debris based on spaceborne single photon radar*. Science Technology and Engineering (2017). 17(10):219–224. doi:10.3969/j.issn.1671-1815.2017.10.038
26. Fu Z, Lin Y. Method to improve accuracy of pulse laser ranging. *Electro-Optic Tech Appl* (2011). 15(2):21–22. doi:10.3969/j.issn.1003-0522.2017.15.010
27. Radar Communication. The relationship between radar parameter measurement accuracy and resolution (2018) Available from: https://www.sohu.com/a/234896120_695278.
28. Lidar. Depth analysis of unmanned lidar (2018) Available from: https://www.sohu.com/a/227001488_100109901.
29. Liu J. *Design and performance study of single-photon detectors based on InGaAs(P)/InP APDs*. Jinan, China: Shandong university (2018).
30. Shangguan M. *Laser remote sensing with 1.5μm single photon detectors*. Hefei, China: University of Science and Technology of China (2017).
31. Liu Y. *Research on multiwavelength dispersion characteristics of optical metasurfaces*. Jinan, China: Shandong university (2019).
32. Qiao J, Mei F, Ye Y. Single-photon emitters in van der Waals materials. *Chin Optic Lett* (2019) 17:020011. doi:10.3788/COL201917.020011
33. Han X, Feng L, Li Y, Zhang L, Song J, Zhang Y. Experimental observations of boundary conditions of continuous-time quantum walks. *Chin Optic Lett* (2019) 17:052701. doi:10.3788/COL201917.052701
34. Amin MZ, Qureshi KK, Hossain MM. Doping radius effects on an erbium-doped fiber amplifier. *Chin Optic Lett* (2019) 17:010602. doi:10.3788/COL201917.010602
35. Lee HJ, Park HS. Generation and measurement of arbitrary four-dimensional spatial entanglement between photons in multicore fibers. *Photon Res* (2019) 7: 19–27. doi:10.1364/PRJ.7.000019
36. Curic D, Giner L, Lundeen JS. High-dimension experimental tomography of a path-encoded photon quantum state. *Photon Res* (2019) 7:A27–A35. doi:10.1364/PRJ.7.000A27
37. Rusby DR, Armstrong CD, Scott GG, King M, McKenna P, Neely D. Effect of rear surface fields on hot, refluxing and escaping electron populations via numerical simulations. *High Power Laser Sci Eng* (2019) 7(3):e45. doi:10.1017/hpl.2019.34
38. Pan KQ, Yang D, Guo L, Li ZC, Li SW, Zheng CY, et al. Enhancement of the surface emission at the fundamental frequency and the transmitted high-order harmonics by pre-structured targets. *High Power Laser Sci Eng* (2019) 7(2):e36. doi:10.1017/hpl.2019.20
39. Yao J. All solid state laser and nonlinear optical frequency conversion technology. Beijing, China: World Sci-Tech R & D (2002) 10 p.
40. Liu X, Deng J, Tang Y. Nonlinear photonic metamaterials. *Materials China* (2019) 38(4):342–51. doi:10.7502/j.issn.1674-3962.2019.04.03
41. Liu X, Tang J, Zhang Y. Nonlinear photonic metamaterials. Available from: https://kc.sustech.edu.cn/handle/2SGJ60CL/62527?mode=full&submit_simple=Show+full+item+record.
42. Sun Y, Duan Y, Cheng M. Triple wavelength-switchable lasing in yellow-green based on frequency mixing of self-Raman operation. *Acta Phys Sin* (2020) 69(12):124201. doi:10.7498/aps.69.20200324
43. Liu P, Wang T. Multi-wavelength thulium-doped mode-locking fiber laser based on nonlinear polarization rotation. *Photon Sin* (2016) 45(6):12–6. doi:10.3788/gzxb20164506.0614003
44. Sroor H, Huang YW, Sephton B. High-purity orbital angular momentum states from a visible metasurface laser. *Nat Photon* (2020) 14:498–503. doi:10.1038/s41566-020-0623-z
45. Eesa R, Kursat S. Femtosecond pulse shaping by ultrathin plasmonic metasurfaces. *J Opt Soc Am* (2016) 33(2):A1–7. doi:10.1364/JOSAB.33.0000A1
46. Xue H, Long L. Orbital angular momentum generation technology and its research progress in the field of radar imaging. Proceedings National antenna conference. Chengdu, China: Antenna Branch of China Electronics Association (2017).
47. Liang C. *Research on the focusing characteristics and application of vortex beams*. Guangzhou, China: South China Normal University (2011).
48. Chen Y, Dong X. Research on radar correlation imaging technology based on orbital angular momentum. *Electron Design Eng* (2018) 6(2): 109–14. doi:10.3969/j.issn.1674-6236.2018.06.024
49. Han J, Intaravanne Y, Ma A, Wang R, Li S, Li Z, et al. Optical metasurfaces for generation and superposition of optical ring vortex beams. *Electron Design Eng* (2020) 14:2000146. doi:10.1002/lpor.202000146

50. Tang D, Chen L, Jia L, Zhang X. Achromatic metasurface doublet with a wide incident angle for light focusing. *Optics Express* (2020) 38:392197. doi:10.1364/OE.392197
51. Kun L, Chase C, Rao Y, Chang-Hasnain CJ. Widely tunable 1060-nm high-contrast grating VCSEL. Compound semiconductor week; 2016 Jun 26–30; Toyama, Japan. IEEE (2016). p. 1–2
52. Bai X. *Application status and prospect of lidar technology*. Beijing, China: Beijing Institute of Technology (2015).
53. Roy T, Zhang S, Jung IW, Troccoli M, Capasso F, Lopez D. Dynamic metasurface lens based on MEMS technology. *APL Photon* (2017) 3: 021302. doi:10.1063/1.5018865
54. Özdemir A, Hayran Z, Takashima Y, Kurt H. Polarization independent high transmission large numerical aperture laser beam focusing and deflection by dielectric Huygens' metasurfaces. *Opt Commun* (2017) 401:46–53. doi:10.1016/j.optcom.2017.05.031
55. Lesina AC, Goodwill D, Eric B, Lora R, Berini P. Optical beam steering for LIDAR via tunable plasmonic metasurface. *IEEE J Sel Top Quant Electron* (2020) 27(1):9166964. doi:10.1109/PN50013.2020.9166964
56. He F, MacDonald KF, Fang X. Continuous beam steering via controlling light with light on a dielectric metasurface. 2019 conference on lasers and electro-optics Europe & European quantum electronics conference; 2019 Oct 17; Munich, Germany. IEEE (2019) 1 p.
57. Xiao J. *Application of metamaterial on beamscanning of microstrip leaky wave antenna*. Chengdu, China: School of Physical Electronics (2015).
58. Qi M. *Manipulations of electromagnetic waves by metamaterial lens and metasurface and their applications*. Nanjing, China: Southeast University (2016).
59. Lin DM, Fan PY, Hasman E, Brongersma ML. Dielectric gradient metasurface optical elements. *Science* (2014) 345(6194):298–302. doi:10.1126/science.1253213
60. Capasso F. Metalenses at visible wavelengths: diffraction-limited focusing and subwavelength resolution imaging. *Science* (2016) 352(6290):1190–4. doi:10.1126/science.aaf6644
61. Shrestha S, Overvig AC, Lu M, Stein A, Yu N. Broadband achromatic dielectric metalenses. *Light Sci Appl* (2018) 7:85. doi:10.1038/s41377-018-0078-x
62. Li T, Chen C, Zhu S. A new method of tomography based on spherical aberration (2019) CN109752842A.
63. Li T, Chen C, Zhu S, Wang S, Zhu S. Optical zoom method based on superstructure lens using wavelength regulation (2018) CN108241208A.
64. Jin M. *Design and implementation of colorful display and metalens based on optical metasurfaces*. Harbin, China: Harbin Industrial University (2019) .
65. Chen K, Feng Y, Monticone F, Zhao J, Zhu B, Jiang T, et al. A reconfigurable active huygens metalens. *Adv Mater* (2017) 29(17):1606422. doi:10.1002/adma.201606422
66. Jia L. *Application of metamaterial in optical transmission*. Nanjing, China: Nanjing University of Aeronautics and Astronautics (2014) .
67. Liu X. Negative refractive index metamaterials to achieve light enhancement eliminate the related research and development of the main obstacles. *Opt Instrum* (2010) 4(1):57–57. doi:CNKI:SUN:GXYQ.0.2010-04-017
68. Zang K, Jiang X, Huo Y, Ding X, Morea M, Chen X, et al. Silicon single-photon avalanche diodes with nano-structured light trapping. *Nat Commun* (2017) 8: 628. doi:10.1038/s41467-017-00733-y
69. Li Q, Gao J, Li Z, Yang H, Liu H, Wang X, et al. Absorption enhancement in nanostructured silicon fabricated by self-assembled nanosphere lithography. *Opt Mater* (2017) 70:165–70. doi:10.1016/j.optmat.2017.05.036
70. Qi H. *Study of nanophotonic structures based perfect absorbers*. Chengdu, China: University of Electronic Science and Technology of China (2015) .
71. Gong L. *The research on irregular nanowire array solar cells*. Beijing, China: Beijing University of Posts and Telecommunications (2016).
72. Zang K, Ding X, Jiang X, Huo Y, Morea M, Chen X, et al. Surface textured silicon single-photon avalanche diode. 2017 conference on lasers and electro-optics (CLEO); 2017 May 14–19; San Jose, CA. IEEE (2017) p. 1–2. Available from: https://ieeexplore.ieee.org/stamp/stamp.jsp?tp=&arnumber=8084082
73. Chen Y. *Research on optimal design and application of perfect absorber based on surface plasmon resonance*. Chengdu, China: China Academy of Engineering Physics (2018).
74. Hoa NTQ, Lam PH, Tung PD, Tuan TS, Nguyen H. Numerical study of a wide-angle and polarization-insensitive ultrabroadband metamaterial absorber in visible and near-infrared region. *IEEE Photon J* (2016) 11(1): 4600208. doi:10.1109/JPHOT.2018.2888971
75. Xu Y, Zhang J, Ai L, Lou X, Lin S, Lu Y, et al. Fabrication of mesoporous double-layer antireflection coatings with near-neutral color and application in crystalline silicon solar modules. *Sol Energy* (2020) 201:149–56. doi:10.1016/j.solener.2020.02.098
76. Ismail Fathima M, Joseph Wilson KS. Efficiency enhancement of silicon solar cell using effective Interface face method in antireflective coating layers. *Int J Mod Phys C* (2020) 31:1–7. doi:10.1142/S012918312050076X
77. Zeng Y, Fan X, Chen J, He S, Yi Z, Ye X, et al. Preparation of composite micro/nano structure on the silicon surface by reactive ion etching: enhanced anti-reflective and hydrophobic properties. *Superlattices Microstruct* (2018) 117: 144–154. doi:10.1016/j.spmi.2018.03.035
78. Chen WH, Hong FCN. 0.76% absolute efficiency increase for screen-printed multicrystalline silicon solar cells with nanostructures by reactive ion etching. *Sol Energy Mater Sol Cells* (2016) 157:48–54. doi:10.1016/j.solmat.2016.05.046
79. Hsueh C-C, Thiyagu S, Liu C-T, Syu H-J, Yang S-T, Lin C-F. Application of silicon nanostructure arrays for 6-inch mono and multi-crystalline solar cell. *Nanoscale Res Lett* (2019) 14:212. doi:10.1186/s11671-019-3030-y

Conflict of Interest: The authors declare that the research was conducted in the absence of any commercial or financial relationships that could be construed as a potential conflict of interest.